



NOVA

University of Newcastle Research Online

nova.newcastle.edu.au

Belova, I. V.; Heuskin, D.; Sondermann, E.; Ignatzi, B.; Kargl, F.; Murch, G. E.; Meyer, A. "Combined interdiffusion and self-diffusion analysis in Al-Cu liquid diffusion couple". *Scripta Materialia* Vol. 143, p. 40-43 (2018)

Available from: <http://dx.doi.org/10.1016/j.scriptamat.2017.09.003>

© 2018. This manuscript version is made available under the CC-BY-NC-ND 4.0 license
<http://creativecommons.org/licenses/by-nc-nd/4.0/>

Accessed from: <http://hdl.handle.net/1959.13/1391763>

Combined Interdiffusion and Self-Diffusion Analysis in Al-Cu Liquid Diffusion Couple

I.V. Belova¹, D. Heuskin², E. Sondermann², B. Ignatzi², F. Kargl², G.E. Murch¹, A. Meyer²

¹University of Newcastle, Australia

²Institut für Materialphysik im Weltraum, Deutsches Zentrum für Luft- und Raumfahrt
(DLR), 51170 Köln, Germany

Abstract

In this paper, a recent combined isotope (tracer) and interdiffusion analysis is adapted to the case of binary liquid alloys. Three shear-cell experiments have been performed recently on liquid Al-Cu that are suitable for demonstration of the application of this analysis. In those experiments, a layer enriched in ⁶⁵Cu was sandwiched between the interdiffusion couple ends. The analysis allows for a generalised treatment of the interdiffusion profile in order to obtain the total flux for one of the components. The self (tracer) diffusion coefficient of Cu is then obtainable as a function of composition in the diffusion zone. Results of the new analysis are in good agreement with an independently measured Cu self (tracer) diffusion coefficient at two compositions.

Keywords: diffusion, interdiffusion experiment, isotopes, metallic alloys, self-diffusion.

1. Introduction

Recently, a combined isotope (tracer) and interdiffusion theoretical approach was developed [1] for application to solid state interdiffusion couples with an addition of an enriched isotope layers in a sandwich-type configuration. The resulting expressions allow for obtaining the self (tracer) diffusion coefficients of the atomic components corresponding to the enriched isotopes. Importantly, these diffusion coefficients are obtained as functions of composition in the diffusion zone.

In liquids, there have been numerous experimental diffusion studies to obtain self-diffusion coefficients [2-19] as well as interdiffusion coefficients [12, 13, 18, 20, 21]. For the measurement of the various diffusion coefficients diverse experimental techniques have been developed [5, 22]. In addition, there has recently been an experimental interdiffusion study [13] of a Al₈₅Ni₁₅ – Al₇₅Ni₂₅ liquid couple where a thin layer of ⁶²Ni isotopes was added between the couple ends with the resulting profile being processed using a Gaussian function analysis. This inevitably gave a constant self-diffusion coefficient for Ni. Furthermore, molecular dynamics simulations were also performed in the same study and excellent agreement was found for the self-diffusion coefficients.

2. Experiment

The shear-cell (in a high temperature isothermal furnace) experimental set up (details are given in [23]) was designed to capture the simultaneous isotope diffusion and interdiffusion process in a liquid Al-Cu diffusion couple. The combined, sandwich type, sequence of phases in the initial state was: Al-Cu10at% – Al-⁶⁵Cu12.5at% – Al-Cu15at%. The stable ⁶⁵Cu isotope was used in the middle layer with an isotope purity of 98.49% (STB Isotope). Pure Al (Alfa Aesar 99.99%) and Cu (Chempur 99.999%) were used as starting materials for the non-isotope parts of the set up. The naturally occurring isotopic composition of Cu (which is 30.83% ⁶⁵Cu and 69.17% ⁶³Cu) was used in the end parts of the diffusion sample. The prepared samples were contained in a large-diameter shear-cell. In total, there were 30 slices, with each slice of the cell being 3mm thick. The sandwich layer consisted of a single slice. In Figure 1 the initial distributions of ⁶⁵Cu, ⁶³Cu and total Cu are presented. The *x*-axis in this Figure corresponds to the vertical axis in the experiment [23] with the left end of the sample being at the top. The setup therefore was such that stable density layering of the liquid column was achieved with more Cu-rich alloys being at the bottom of the cell [24]. During heating and melting the shear-cell was kept horizontal for homogenisation of the separated samples constituting the diffusion couple. Prior to the shear, at the target temperature of 973K, the cell was moved to an upright position. The diffusion was initiated by shearing the middle disc containing the enriched ⁶⁵Cu layer. The diffusion process was stopped after a pre-selected annealing time (2 hours) by shearing every-other disc by 30 degrees. As a result, the liquid column was separated into individual liquid slices. Subsequently, the setup was cooled to room temperature and the individual slices solidified. The analysis of the resulting composition profiles was achieved by fully dissolving the individual slices and subsequently analysing them by means of atomic absorption spectroscopy (AAS, Varian AA240FS) and inductively-coupled plasma mass spectroscopy (ICP-MS, Varian 820-MS).

In total, three experiments were carried out simultaneously, of which Exp 1 was considered to have been the best one. Up to the present, the recently developed combined isotope and interdiffusion analysis [1] has not been applied to diffusion in a liquid alloy. Therefore, in this study, we will analyse these three experiments.

In Figs. 2 and 3 we present results of this analysis for all three experiments. In Figure 2, the total interdiffusion profile of c_{Cu} is presented as a function of diffusion distance. In Figure 3 the fraction of ⁶⁵Cu of the total Cu is presented as well. The distribution of this fraction is much smoother than the corresponding total Cu distribution in all three experiments. This is due to

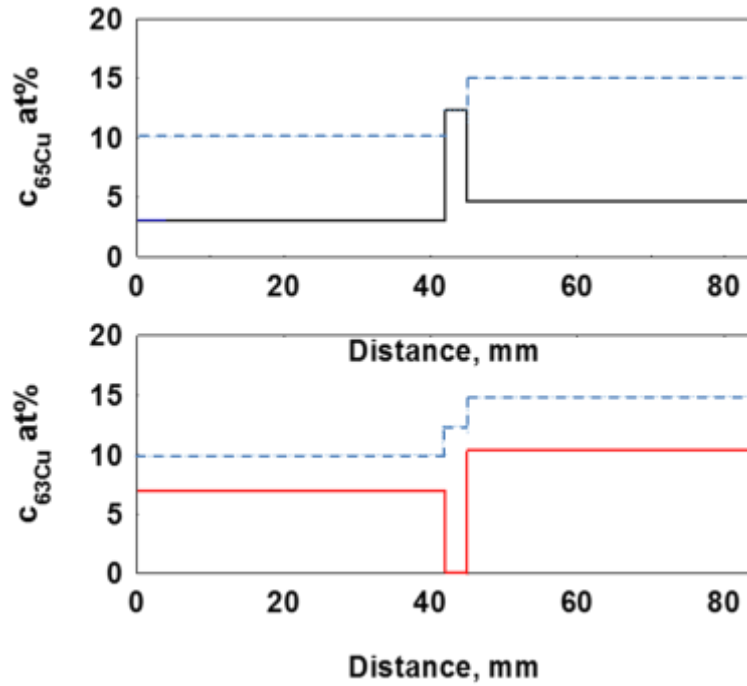


Figure 1. Initial compositional profiles for isotopes ^{65}Cu and ^{63}Cu . The initial total Cu (blue dashes line) composition profile has a two-step shape.

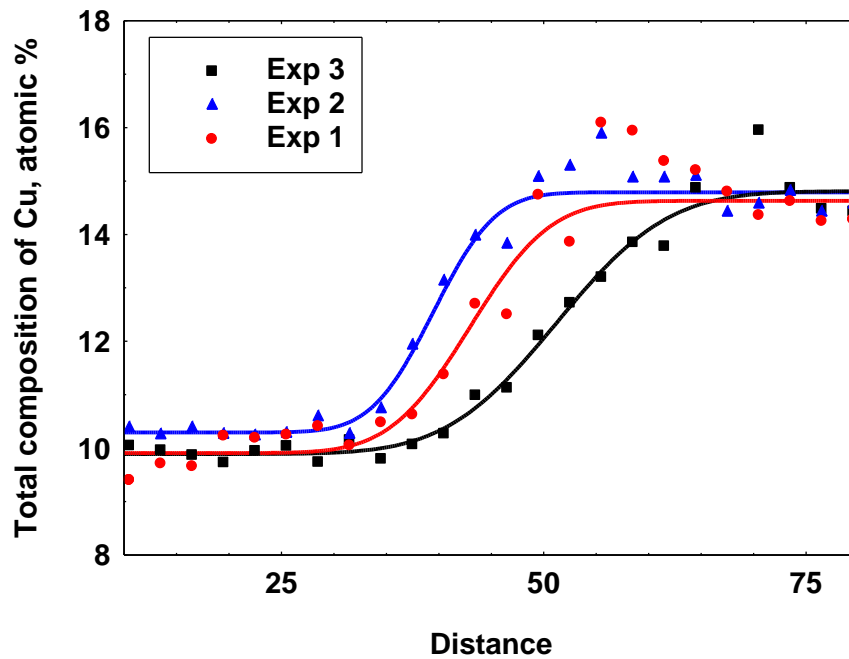


Figure 2. Interdiffusion composition profiles, c_{Cu} , measured by AAS in three simultaneously processed Al-Cu liquid sandwich-type diffusion couples. The shift in the data (blue triangles and black squares) is due to the graphite-felt volume compensation mechanism acting statistically differently on the capillaries. The shift is \pm one slice along the axial direction.

the lower statistical error in ICP-MS compared with AAS analysis. This smoother curve allows for successful application of the simultaneous isotope and interdiffusion analysis described in the next section for the case of liquid alloys.

In the same Figure 3 we have plotted the Gaussian functions fitted to the data points. Under the assumption that the diffusion of ^{65}Cu is not affected by the interdiffusion process, a back-to-back error functions solution (see, for example, [25]) can also be fitted to these ratios to obtain the corresponding constant self- (or tracer) diffusion coefficients. In the section on the error analysis below we show that the back-to-back error functions solution converges to the Gaussian distribution at long enough anneal times.

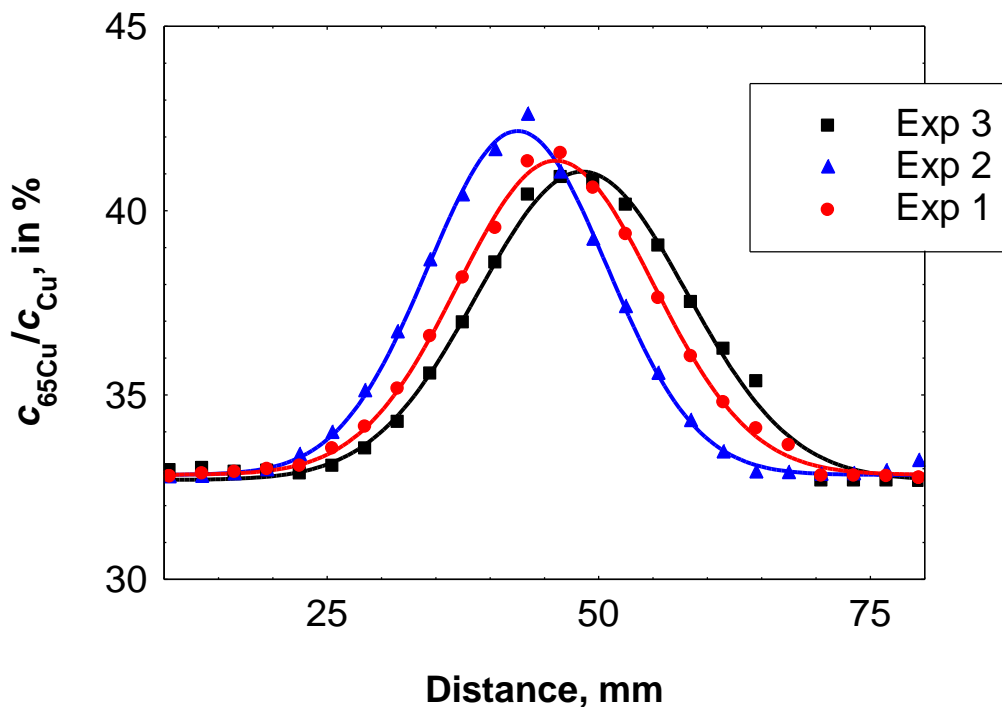


Figure 3. Ratio of $c_{65\text{Cu}}/c_{\text{Cu}}$ (in %) for the same three diffusion couples as in Figure 2 measured by ICP-MS as function of diffusion distance. Symbols represent experimental data. Solid lines are the Gaussian solution fits.

3. Theory

In [1] the analytical formalism of the simultaneous interdiffusion and self-diffusion experiment for solid state multicomponent alloys was derived. For completeness, we will briefly present this derivation here for the case of liquid alloys.

We consider a binary liquid alloy Al-Cu with Cu having two stable isotopes, ^{65}Cu and ^{63}Cu . First, we assume that the mean-volume reference frame coincides with the laboratory

reference frame, which is correct in the case of a constant number of atoms per unit volume. Second, we assume that in the laboratory reference frame the atomic fluxes (= number of corresponding type of atoms crossing a unit area per unit time) can be presented by the Onsager expressions of non-equilibrium thermodynamics:

$$J_i = \sum_{j=1}^n L_{ij} X_j \quad (1)$$

where L_{ij} are the Onsager transport (phenomenological) coefficients, the X_j are the forces acting on atoms of type j .

In the liquid interdiffusion experiment, we consider thermodynamic forces and additional drift producing forces G_i :

$$X_i = -\nabla\mu_i + G_i \quad (2)$$

where $\nabla = \partial/\partial x$, and x is the diffusion direction, μ_i is the chemical potential of the atomic species i . We will not speculate about the nature of the G_i forces, but will assume that G_i typically are much smaller than the thermodynamic forces. (Ideally, they should be completely suppressed for diffusion experiments in liquids.) Furthermore, we assume that G_i are functions of composition only and that they are the same for isotopes of the same atomic component.

For the thermodynamic parts of the forces, we have that [26]:

$$-\nabla\mu_{Ai} = -\nabla[\mu_{0A}(T, P) + kT\ln(c_{Ai}\gamma_A)] = -kT[\nabla c_{Ai}/c_{Ai} + \nabla\ln(\gamma_A)], \quad i = 1, 2; \quad (3)$$

$$-\nabla\mu_A = -\nabla[\mu_{0A}(T, P) + kT\ln(c_A\gamma_A)] = -kT(\nabla\ln(\gamma_A) + \nabla c_A/c_A). \quad (4)$$

where γ_A is the activity coefficient of the A component and which depends on the total composition of A atoms, but not on the composition of isotopes A1 and A2 separately. In writing Eqs. 3 and 4 we have labelled natural Cu as A, the two isotopes of Cu as A1 and A2 (with their respective atomic fraction compositions as $c_{A1} + c_{A2} = c_A$, the natural occurrences of the ^{65}Cu and ^{63}Cu are 30.83% and 69.17% respectively). In what follows, A1 will be labelled as B.

We will consider an initial geometric configuration in which a very thin layer of alloy with an intermediate composition but with only the isotope A1 being placed between the two parts of the diffusion couple (Figure 1).

The next part of the derivation follows [1]. Explicit Onsager expressions (Eqs. 1) for the atomic fluxes in the laboratory coordinate system are:

$$J_{A1} = L_{A1A1}X_{A1} + L_{A1A2}X_{A2} + L_{A1B}X_B, \quad J_{A2} = L_{A1A2}X_{A1} + L_{A2A2}X_{A2} + L_{A2B}X_B \quad (5)$$

$$J_B = L_{A1B}X_{A1} + L_{A2B}X_{A2} + L_{BB}X_B \quad (6)$$

We will need the following obvious relations as well:

$$J_A = J_{A1} + J_{A2} \quad (7)$$

$$c_A X_A = c_{A1} X_{A1} + c_{A2} X_{A2} \quad (8)$$

We will now use the following exact relations derived from linear response theory [27] for the Onsager coefficients:

$$L_{A1A1} = \frac{Nc_{A1}}{kT} (D_A^* + c_{A1}F_A), \quad L_{A2A2} = \frac{Nc_{A2}}{kT} (D_A^* + c_{A2}F_A), \quad L_{A1A2} = L_{A2A1} = \frac{Nc_{A1}c_{A2}}{kT} F_A, \\ L_{AA} = \frac{Nc_A}{kT} (D_A^* + c_A F_A), \quad (9)$$

$$L_{BB} = \frac{Nc_B}{kT} (D_B^* + c_B F_B), \quad L_{A1B} = \frac{Nc_{A1}c_B}{kT} F_{AB}, \quad L_{A2B} = \frac{Nc_{A2}c_B}{kT} F_{AB}, \quad (10)$$

where D_A^* , D_B^* are the self or tracer diffusion coefficients of atoms A and B respectively, $F_{A(B)}$ is a function reflecting correlation between the movements of two different A(B) atoms and F_{AB} is a function reflecting cross-correlation between the movements of A and B atoms. F_A and F_{AB} are the same for all A atom isotopes, N is the total number of atoms per unit volume and it is assumed to be constant in this study.

Applying Eqs. 7 - 10 to the right hand sides of Eqs. 5 and 6 we soon have that:

$$J_{A1} = \frac{N}{kT} D_A^* c_{A1} (X_{A1} - X_A) + \frac{c_{A1}}{c_A} J_A; \quad (11)$$

and similarly for J_{A2} .

Using the assumption that the drift forces for all isotopes of A atoms are equal, $G_{A1} = G_{A2} = G_A$, and Eqs. 3 and 4 for the thermodynamic forces, we have for J_{A1} :

$$J_{A1} = -ND_A^* \left(\nabla c_{A1} - \frac{c_{A1}}{c_A} \nabla c_A \right) + \frac{c_{A1}}{c_A} J_A; \quad (12)$$

and similarly for J_{A2} .

Eqs. 12 can be used to extract the self-diffusion coefficient D_A^* when the interdiffusion composition profiles for total A and for one of the isotopes are known. It is obvious that this is possible only in a specially designed interdiffusion experiment where [1]

$$\nabla c_{A2} - \frac{c_{A2}}{c_A} \nabla c_A \neq 0. \quad (13)$$

The corresponding Diffusion Equations (Fick's Second Law) for A1 and A are:

$$\frac{\partial c_{A1}}{\partial t} = -\nabla J_{A1}/N = \nabla \left[D_A^* \left(\nabla c_{A1} - \frac{c_{A1}}{c_A} \nabla c_A \right) - \frac{c_{A1}}{c_A} J_A/N \right]; \quad (14)$$

$$\frac{\partial c_A}{\partial t} = -\nabla J_A/N = \nabla (\tilde{D} \nabla c_A) \quad (15)$$

where t is the time variable, ∇ is the gradient along the space variables, \tilde{D} is the interdiffusion coefficient (sometime this coefficient is denoted by D_{AB}) that can be expressed in terms of the phenomenological coefficients and thermodynamic factor ϕ as:

$$\tilde{D} = \phi \frac{kT}{N} \left(\frac{c_B}{c_A} L_{AA} + \frac{c_A}{c_B} L_{BB} - 2L_{AB} \right) \quad (16)$$

We can now apply this theory to the interdiffusion experiment described in the previous section. We assume that the width of the intermediate layer (3mm) is small enough compared to the interdiffusion length, $2\sqrt{\tilde{D}t}$. With this assumption, the diffusion spread of the intermediate (the isotopes) layer can be considered to follow the functional form $g(\lambda)/\sqrt{t}$, where $\lambda = x/\sqrt{t}$ is the Boltzmann variable. Then, the Cu self-diffusion coefficient can be estimated by the following solution derived in [1] (note that c_{A1} is defined as the excess of the isotopes A1 above the natural occurrence for this solution to be valid)

$$D_{Cu}^* = - \left(\frac{(x+a)}{2t} + \tilde{D} \frac{d \ln c_A}{dx} \right) / \left(\frac{d \ln(c_{A1}/c_A)}{dx} \right) \quad (17)$$

or, the more general form:

$$D_{Cu}^* = - \left(\frac{(x+a)}{2t} - \frac{J_A/N}{c_A} \right) / \left(\frac{d \ln(c_{A1}/c_A)}{dx} \right) \quad (18)$$

The parameter a (appearing here as an integration constant) can be identified using the following method: first, the derivative function $\frac{d \ln(c_{A1}/c_A)}{dx}$ should be calculated as a function of composition in the diffusion zone; this function will go through zero at some composition $\{x', c'_{A1}\}$. Next, the numerator function $\frac{(x+a)}{2t} + \tilde{D} \frac{d \ln c_A}{dx}$ should be calculated at the same point $\{x', c'_{A1}\}$, then equating this function to zero and solving it w.r.t. the parameter a will finish the search.

Eq. 17 should be used if the drift forces G_i are negligibly small and the interdiffusion coefficient \tilde{D} can then be obtained from the analysis of the profile for the total A(B) atoms composition by making use of a standard analysis, for example, Sauer-Freise [28] or simply an error function solution when \tilde{D} is assumed to be independent of composition. If, on the other hand, Eq. 18 is used, the flux J_A^0/N , in general, can be calculated using the following expression [28]:

$$J_A/N = \frac{c_A^+ - c_A^-}{2t} \times \left[(1 - y_A^*) \int_{-\infty}^{x^*} y_A dx + y_A^* \int_{x^*}^{\infty} (1 - y_A) dx \right] \quad (19)$$

where x^* is the point of evaluation, $y_A = (c_A - c_A^-)/(c_A^+ - c_A^-)$ is the scaled mole fractions of atoms A and the superscripts “+” and “-” denote the right and left hand ends of the diffusion couple.

In our analysis below, we will use Eq. 17.

4. Analysis of the experiment

In application of Eq. 17 to the experimental data (Figs. 2 and 3), as was already specified above, the A atoms are Cu, the A1 atoms consist of the excess of the isotope ^{65}Cu above its natural occurrence level, the B atoms are Al . The end compositions are: $c_{Cu}^- = 0.10$; $c_{Cu}^+ = 0.15$. Traditional interdiffusion analysis always consists of two parts, the integration part of the interdiffusion profile and the derivative part of the same interdiffusion profile. Both parts are implemented numerically on the discrete set of experimentally obtained compositional points. The integration part is relatively insensitive to the experimental error, in contrast with

the derivative part, which is very sensitive to the experimental error. To minimise the effect of this error, the interdiffusion profile is usually carefully smoothed out. In the case of the present analysis, it is clear that the interdiffusion profile (Figure 2) should be used for error function fitting with the assumption that the interdiffusion coefficient is constant. This will be used for the integration part of the analysis (to calculate $\tilde{D} \frac{d \ln c_A}{dx}$). The derivative part now has to be applied to a different type of profile. In fact, it involves the derivative of the ratio $(c_{65Cu} - kc_{Cu})/c_{Cu}$, where $k = 0.3083$ (the natural occurrence of ^{65}Cu). In Figure 3 the ratio c_{65Cu}/c_{Cu} is presented for all three experiments and it can be used (minus k) in the right hand side in Eqs. 17. It should be noted that, fortunately, this ratio is much smoother than the total composition of Cu (Figure 2). Furthermore, the Gaussian distribution (solid lines in Figure 3) works very well as a smoothing function.

We can safely assume that the forces G_i are all negligibly small and then the interdiffusion profile has an error function shape (when the interdiffusion coefficient is independent of composition). The appropriate error function together with the corresponding interdiffusion coefficient \tilde{D} should then be identified and used for the term $\tilde{D} \frac{d \ln c_A}{dx}$ in Eq. 17. We will apply our analysis to the experimental profiles and compare the results for the self-diffusion coefficients with available data measured by the quasi-elastic neutron scattering (QENS) technique [29].

5. Results

In the first experiment, the best fit was achieved with the interdiffusion coefficient: $2.5 \times 10^{-9} \text{ m}^2/\text{s}$. Similarly, for the second experiment and the third experiment we have $1.5 \times 10^{-9} \text{ m}^2/\text{s}$; and $4.8 \times 10^{-9} \text{ m}^2/\text{s}$ correspondingly. These best fits (shown in Figure 2 with solid lines) were done using the error function solution [25]. Due to the uncertainty in concentration measurements, there is a large uncertainty of up to $\pm 1.6 \times 10^{-9} \text{ m}^2/\text{s}$.

In Figure 4 we show results of the application of Eq. 17 to the interdiffusion profiles and the ratios $(c_{65Cu} - kc_{Cu})/c_{Cu}$, (Figs. 2 and 3). For all three experiments the resulting self-diffusion coefficients, shown by solid lines, slightly decrease with an increase in concentration.

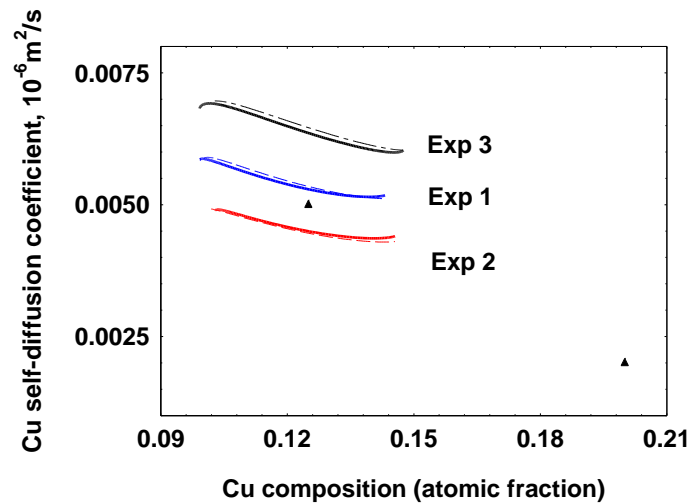


Figure 4. Results of combined isotopic and interdiffusion analysis where a constant interdiffusion coefficient and corresponding error function for the interdiffusion profile were assumed. The Cu self-diffusion coefficient was calculated for all three experiments as a function of composition. The triangles represent results of independent QENS measurements on AlCu12.5at% [29] and AlCu20at% [20].

The results of Experiment 1 give a very good agreement with the independently measured self-diffusion coefficient of AlCu12.5at%. Experiment 2 underestimates the diffusion coefficient by about 10% and Experiment 3 overestimates the self-diffusion coefficient by about 20%. The overestimation of the self-diffusion coefficient goes along with an interdiffusion coefficient, which is about 25% larger than the accurate value. The increased value agrees well with *in-situ* X-ray radiography measurements that showed a similar increase in the apparent interdiffusion coefficient due to Marangoni flow [24]. Underestimation of the values can typically occur in the case of diffusion barriers. This might be the case in Experiment 2.

In addition, it should be noted that the self-diffusion coefficients (Figure 4) calculated as functions of composition have characteristic (slight) initial downward and final upward curvatures. This is usually accepted as the indication that the diffusion coefficient is becoming less reliable. This happens at the tails of the corresponding composition profiles where the intrinsic experimental error is the highest. These parts are usually not truncated and left for the reader to decide on the reliability range. In the case of Figure 4, it can be concluded that the Cu self-diffusion coefficient decreases almost linearly between 10 to 14 at% of Cu.

6. Error Analysis

The main error sources are: experimental measurements uncertainty and the main assumptions for the developed analysis. The other error sources: finite couple interdiffusion experiment (an infinite couple is assumed in the analysis), two-step initial composition distribution (one-step initial composition is assumed in the analysis), a volume change during the interdiffusion process.

Using Figure 2, the experimental error can be estimated by the amount of the final Cu composition fluctuations at the left and right ends of the couple. The above mentioned large uncertainties of fitting the error function solution (solid lines in Figure 2) into the interdiffusion profiles, surprisingly, do not affect much the resulting self-diffusion coefficients as functions of compositions. For example, in Figure 4, solid lines corresponds to results with the interdiffusion coefficients taken from the best fits, dashed lines corresponds to the interdiffusion coefficients taken at their upper limits.

Next, let us consider the main assumption in the developed analysis, that the sandwiched layer is thin enough for the application of the shifted Gaussian type function to the resulting spread of the layer. The correct solution for the spread of the thick layer is a two-error function (back-to-back error functions) solution. The condition for the two-error function solution being close enough to the Gaussian solution is:

$$h^2 / 4Dt \ll 1.0 \quad (20)$$

which is satisfied if

$$h / (Dt)^{1/2} < 2.0 \quad (21)$$

This is valid at the final stages of the experiment ($h = 3\text{mm}$, $Dt = 36\text{mm}^2$), therefore the middle part of the Gaussian solution should be satisfactory, and the “tails” would have to show some deviations (hopefully small) from it. This is an important condition for applying the developed analysis because it is based on Gaussian solutions for the sandwiched part of the composition.

We have checked the effect of a changing molar volume using data from [30]. This effect is insignificant for the concentration variations involved. The molar volume maximum change is about 0.2%, which is impossible to detect and is well below the interdiffusion experiment error.

The finite couple effect has been checked numerically on a few model systems and for the parameters chosen for the experiment this effect is absolutely negligible. Similarly, for the two-step initial composition distribution, the deviation from the analysis due to this effect is controlled by the above condition Eqs. 20, 21.

7. Conclusions

In this paper, a combined isotope (tracer) and interdiffusion analysis has been adapted to the case of liquid alloys. It was then applied to analyse self (tracer) diffusion coefficients in a AlCu alloy at compositions between 10at% and 15at% of Cu. In total, three experiments have been performed and analysed. In those experiments, a layer enriched in ^{65}Cu was sandwiched between the interdiffusion couple ends. The new analysis allows for taking into account the influence of the total flux of the components on the isotope diffusion process. The self (tracer) diffusion coefficient of Cu was obtained as a function of composition in the diffusion zone. The new analysis were found to be in good agreement with an independently measured Cu self (tracer) diffusion coefficient at two compositions.

Acknowledgments

IVB, GEM and AM wish to thank the Australian Research Council for its support of this research under the Discovery Project Grants Scheme (DP130101464).

References

- [1] I.V. Belova, Y.H. Sohn and G.E. Murch, Measurement of Tracer Diffusion Coefficients in an Interdiffusion Context for Multicomponent Alloys, *Philosophical Magazine Letters*, **95**, (2015) 416-424.
- [2] N. H. Nachtrieb, J. Petit, Self-Diffusion in Liquid Mercury, *J Chem Phys* **24** (1956) 746.
- [3] L. Yang, M. T. Simnad, G. Derge, *Trans AIME* **209** (1957) 1577.
- [4] J. Henderson, L. Yang, *Trans AIME* **221** (1961) 72.
- [5] T. Iida, R. I. L. Guthrie, *The Physical Properties of Liquid Metals*. Oxford: Clarendon Press, 1993.
- [6] G. Mathiak, A. Griesche, K. H. Kraatz, G. Froberg, Diffusion in liquid metals, *J Non-Cryst Solids* **205** (1996) 412.
- [7] A. Meyer, S. Stuber, D. Holland-Moritz, O. Heinen, T. Unruh, Determination of self-diffusion coefficients by quasielastic neutron scattering measurements of levitated Ni droplets, *Phys Rev B* **77** (2008) 092201.
- [8] A. Meyer, Self-diffusion in liquid copper as seen by quasielastic neutron scattering, *Phys Rev B* **81** (2010) 012102.
- [9] F. Kargl, H. Weis, T. Unruh, A. Meyer, Self diffusion in liquid aluminium, *J Phys: Conf Series* **340** (2012) 012077.
- [10] A. Bruson, M. Gerl, Diffusion coefficients of ^{124}Sb , ^{113}Sn , ^{110}mAg , and ^{195}Au in liquid copper, *Phys Rev B* **19** (1979) 6123.
- [11] A. Bruson, M. Gerl, Diffusion coefficient of ^{113}Sn , ^{124}Sb , ^{110}mAg , and ^{195}Au in liquid Sn, *Phys Rev B* **21** (1980) 5447.
- [12] A. Griesche, M.P. Macht, G. Froberg, Chemical diffusion in bulk glass-forming Pd₄₀Cu₃₀Ni₁₀P₂₀ melts, *Script Mat* **53** (2005) 1395.
- [13] J. Horbach, D. K. Das, A. Griesche, M. P. Macht, G. Froberg, A. Meyer, Self-diffusion and interdiffusion in Al₈₀Ni₂₀ melts: Simulation and experiment, *Phys Rev B* **75** (2007) 174304.

- [14] S. Stüber, D. Holland-Moritz, T. Unruh, A. Meyer, Ni self-diffusion in refractory Al-Ni melts, *Phys. Rev. B* **81**, 024204 (2010).
- [15] F. Kargl, M. Engelhardt, F. Yang, H. Weis, P. Schmakat, B. Schillinger, A. Griesche, A. Meyer, In situ studies of mass transport in liquid alloys by means of neutron radiography, *J. Phys.: Condens Matter*, **23**, 254201(2011).
- [16] H. Weis, T. Unruh, A. Meyer, The measurement of self-diffusion coefficients in liquid Germanium using quasielastic neutron scattering, *High Temp. High Press.* **42**, 39 (2013).
- [17] A. Meyer, F. Kargl, Diffusion of Mass in Liquid Metals and Alloys - Recent Experimental Developments and New Perspectives, *J. Jpn. Soc. Microgravity Appl.* **30**, 30 (2013).
- [18] P. Kuhn, J. Horbach, F. Kargl, A. Meyer, T. Voigtmann, Diffusion and interdiffusion in binary metallic melts, *Phys. Rev. B* **90**, 024309 (2014).
- [19] F. Yang, D. Holland-Moritz, J. Gegner, P. Heintzmann, F. Kargl, C. C. Yuan, G. G. Simeoni, A. Meyer, Atomic dynamics in binary Zr-Cu liquids, *EPL*, **107**, 46001 (2014).
- [20] B. Zhang, A. Griesche, A. Meyer, Diffusion in Al-Cu Melts Studied by Time-Resolved X-Ray Radiography, *Phys Rev Lett* **104** (2010) 035902.
- [21] A. Griesche, M. P. Macht, G. Froberg, First results from diffusion measurements in liquid multicomponent Al-based alloys, *J Non-Cryst Solids* **353** (2007) 3305.
- [22] Y. Du, L. J. Zhang, S. L. Cui, D. D. Zhao, D. D. Liu, W. B. Zhang, W. H. Sun, W. Q. Jie, Atomic mobilities and diffusivities in Al alloys, *Sci China Tech Sci* **55** (2012) 306.
- [23] D. Heuskin, F. Kargl, A. Griesche, Ch. Stenzel, D. Mitschke, D. Brauer and A. Meyer, MSL compatible isothermal furnace insert for high temperature shear-cell diffusion experiments, *Journal of Physics: Conference Series*, **327** (2011) 012053.
- [24] F. Kargl, E. Sondermann, H. Weis, A. Meyer, Impact of convective flow on long-capillary chemical diffusion studies of liquid binary alloys, *High Temp. High Press.* **42**, 1 (2013).
- [25] J. Crank, *The Mathematics of Diffusion*. New York: Oxford University Press, 1975.
- [26] R.E. Howard and A.B. Lidiard, Matter transport in solids, *Rep. Prog. Phys.* **27** (1964) p. 161.
- [27] A.R. Allnatt and A.B. Lidiard, *Atomic Transport in Solids*, Cambridge University Press, 1993, pp 227-233.
- [28] F. Sauer, V. Freise, Diffusion in binären Gemischen mit Volumenänderung, *Z. Elektrochem* **66** (1962) 353.
- [29] Paper in preparation.
- [30] J.Brillo, I. Egry, Density of Multicomponent Melts Measured by Electromagnetic Levitation, *Japanese Journal of Applied Physics*, **50** (2011) 11RD02.